Engineering Analysis with Boundary Elements 73 (2016) 133–143

Contents lists available at ScienceDirect

Engineering Analysis with Boundary Elements

journal homepage: www.elsevier.com/locate/enganabound

Three-dimensional BEM analysis of stress state near a crack-borehole system

Dmitry V. Nikolskiy[a], Mattia Zammarchi[b,1], Sofia G. Mogilevskaya[a,*], Alberto Salvadori[b,c,d]

[a] Department of Civil, Environmental, and Geo-Engineering, University of Minnesota, 500 Pillsbury Drive S.E., Minneapolis, MN 55455, USA
[b] DICATAM - Department of Civil, Environmental, Architectural Engineering and Mathematics, University of Brescia, via Branze 43, 25123 Brescia, Italy
[c] Department of Aerospace and Mechanical Engineering, University of Notre Dame, 365 Fitzpatrick Hall, Notre Dame, IN 46556, USA
[d] Center for Shock Wave-processing of Advanced Reactive Materials, University of Notre Dame, 117 Cushing Hall, Notre Dame, IN 46556, USA

ARTICLE INFO

Keywords:
Hydraulic fracturing
Boundary element method
Numerical simulations

ABSTRACT

The paper presents a numerical study of the three-dimensional problem of cracks interacting with a cylindrical uniformly pressurized borehole. The theoretical developments describe general case in which the axis of the borehole can be inclined to the vertical direction, the cracks are either located outside of the borehole or emanate from it, and the in-situ stresses are uniform with major principal stress acting in vertical direction. The tractions are prescribed at the cracks surfaces that includes two limiting cases of traction-free cracks ("fast pressurization") or cracks subjected to uniform load equal to that applied at the surface of the borehole ("slow pressurization"). The study is based on the complex integral representations for the three-dimensional fields around the borehole-crack system. The boundary surfaces are approximated using triangular mesh and quadratic polynomials are employed for approximating the boundary unknowns. The prescribed boundary conditions are met using "limit after discretization" procedure. The linear algebraic system to find the unknowns is set up by the collocation method. Two numerical benchmarks are presented.

1. Introduction

The problem of borehole-crack interaction is important for the analysis of different scenarios of crack propagation during hydraulic fracturing process. Two-dimensional studies of such systems are reported in several publications, see e.g [1–6] and the references therein, however, fewer simulations are done in three-dimensional settings mostly using Finite Element Method, e.g. [7–10] and the references therein.

In this paper we investigate the three-dimensional problem of borehole-cracks interaction using the boundary element technique presented in [11]. The technique developed in [11,12] for crack problems is based on the use of exact boundary integral representations of the elastic fields. In [11], an efficient numerical procedure was suggested to solve the problem and find the unknown parameters involved in these integral representations. The procedure employed triangular elements to approximate crack surfaces and used complex variables for various combinations of the fields, e.g. in-plane components of tractions, displacement discontinuities, as well as geometric parameters. Other important features of the technique included analytical integration over the elements, "limit after discretization" procedure to enforce the boundary conditions after the discretization, and collocation procedure to set up linear algebraic system and find the unknown boundary parameters. Using this procedure, in [11], closed-form analytical expressions were provided for the stresses and tractions everywhere in the computational domain.

Here, we extend this technique to explicitly include the borehole in the system. In the present study, we assume that the borehole is uniformly pressurized and, in general, can be inclined to the vertical direction. The cracks can be located either outside of the borehole or emanate from it, and the in-situ stresses are uniform with major principal stress acting in vertical direction. The cracks' surfaces are assumed to be subjected to prescribed tractions.

The integral representation of this problem includes an additional integral term (potential, see [13,14]) related to the boundary of the borehole; this potential produces a host of additional integrals. In the present paper, these integrals are evaluated analytically using the technique reported in [15]; the computational algorithm of [11] is further modified to incorporate this new potential. Special attention is paid to the case of cracks emanating from the borehole, which requires careful handling of the crack mouth. The parallelization procedure is used in the assembly of the matrix of the system of algebraic equation

* Corresponding author.
E-mail address: mogil003@umn.edu (S.G. Mogilevskaya).
[1] The work was performed during an internship at the Department of Civil, Environmental, and Geo-Engineering, University of Minnesota.

http://dx.doi.org/10.1016/j.enganabound.2016.09.007
Received 2 June 2016; Received in revised form 12 September 2016; Accepted 12 September 2016

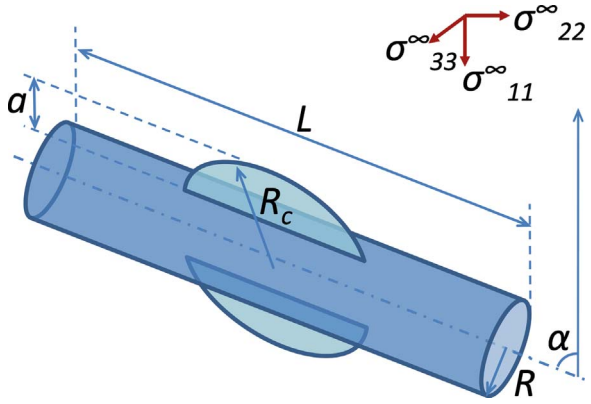

Fig. 1. An example of borehole-crack system.

to reduce computational time. Three numerical benchmark examples of a borehole and the cracks emanating from that borehole (for "fast" and "slow" pressurization) are presented to validate the approach.

2. Problem formulation

Consider a homogeneous elastic isotropic medium with a cylindrical hole of radius R and length L, representing a borehole. It is assumed that, in general, the axis of the borehole is inclined to the vertical direction by the angle α. Uniform pressure P is applied to the boundary of the borehole and uniform loads σ_{11}^{∞}, σ_{22}^{∞}, σ_{33}^{∞} are applied at infinity. The cracks are either located outside of the borehole or emanate from it (see, e.g., Fig. 1 for the latter case).

The tractions are assumed to be prescribed at the cracks surfaces. That includes two limiting cases: traction free cracks ("fast pressurization"), or cracks subjected to uniform load P equal to that applied at the surface of the borehole ("slow pressurization"). The elastic fields around the borehole-crack system need to be investigated.

2.1. Integral representations

The displacements at a certain point $\mathbf{x}$ outside of the crack-borehole boundaries can be represented by the following Somigliana's identity [16]:

$$u_j(\mathbf{x}) = u_j^{\infty}(\mathbf{x}) + \int_S U_{jk}(\mathbf{x}, \boldsymbol{\xi}) t_k(\boldsymbol{\xi}) dS_{\xi} - \int_S T_{kj}(\boldsymbol{\xi}, \mathbf{x}) \Delta u_k(\boldsymbol{\xi}) dS_{\xi} \tag{1}$$

where $u_j(\mathbf{x})$ is the j-th component of the displacement vector at the point $\mathbf{x}$ in the arbitrary chosen Cartesian coordinate system, $u_j^{\infty}(\mathbf{x})$ is j-th component of the linear displacements due to the uniform far-field stresses, $S = S_b \cup S_c$, S_b is the surface of the borehole, S_c is the totality of the cracks' surfaces, t_k is the k-th components of the traction vector $\mathbf{t}(\boldsymbol{\xi})$ at the point $\boldsymbol{\xi} \in S$; $\Delta u_k(\boldsymbol{\xi}) = u_k(\xi)^+$ for $\boldsymbol{\xi} \in S_b$; $\Delta u_k(\boldsymbol{\xi}) = u_k(\xi)^+ - u_k(\boldsymbol{\xi})^-$ for $\boldsymbol{\xi} \in S_c$, where the opposite sides of the crack are denoted with "+" and "-". $U_{jk}(\mathbf{x}, \boldsymbol{\xi})$ and $T_{kj}(\boldsymbol{\xi}, \mathbf{x})$ are the following components of tensors $\mathbf{U}$ and $\mathbf{T}^T$ (Kelvin's fundamental solutions) that are involved in the so-called single and double layer potentials, see [13,14,16,17]:

$$U_{jk}(\mathbf{x}, \boldsymbol{\xi}) = \frac{\beta}{\mu r}\left[(3 - 4\nu)\delta_{jk} + \frac{r_j r_k}{r^2}\right] \tag{2}$$

$$T_{jk}(\mathbf{x}, \boldsymbol{\xi}) = \frac{2(1 - 2\nu)\beta}{r^3}[n_j(\mathbf{x}) r_k - r_m n_m(\mathbf{x})\delta_{jk} - r_j n_k(\mathbf{x})] - \frac{6\beta}{r^5} r_j r_m n_m(\mathbf{x}) r_k \tag{3}$$

in which δ_{jk} is Kronecker's symbol, $r_k = x_k - \xi_k$, $r = |\mathbf{x} - \boldsymbol{\xi}|$, $\beta = \frac{1}{16\pi(1-\nu)}$, μ is the shear modulus, ν is Poisson's ratio, and $\mathbf{n}(\mathbf{x})$ is the outward unit normal vector at the point $\mathbf{x}$; $n_k(\mathbf{x})$ is its k-th component. Note that $T_{kj}(\boldsymbol{\xi}, \mathbf{x})$ can be obtained from $T_{jk}(\mathbf{x}, \boldsymbol{\xi})$ by substituting $-r_j$ for r_j and $n_k(\boldsymbol{\xi})$ for $n_k(\mathbf{x})$, where $n_k(\boldsymbol{\xi})$ is the k-th component of the outward unit normal vector $\mathbf{n}(\boldsymbol{\xi})$ at the boundary point $\boldsymbol{\xi}$. For $\boldsymbol{\xi} \in S_c$, $\mathbf{n}(\boldsymbol{\xi})$ is the outward unit normal vector to the side identified by the "+" sign.

Using Eq. (1), strain-displacements relations, and Hooke's law, the tractions at the point $\mathbf{x}$ outside of the surface S on the plane characterized by the normal vector $\mathbf{n}(\mathbf{x})$ can be obtained

$$t_j(\mathbf{x}) = t_j^{\infty}(\mathbf{x}) + \int_S T_{jk}(\mathbf{x}, \boldsymbol{\xi}) t_k(\boldsymbol{\xi}) dS_{\xi} - \int_S H_{jk}(\mathbf{x}, \boldsymbol{\xi}) \Delta u_k(\boldsymbol{\xi}) dS_{\xi} \tag{4}$$

where $t_j^{\infty}(\mathbf{x}) = \sigma_{jk}^{\infty}(\mathbf{x}) n_k(\mathbf{x})$ is j-th component of the tractions due to the far-filed stresses, and the components $H_{jk}(\mathbf{x}, \boldsymbol{\xi}) = H_{kj}(\boldsymbol{\xi}, \mathbf{x})$ of the hypersingular kernel $\mathbf{H}$ are as follows:

$$\begin{aligned} H_{jk}(\mathbf{x}, \boldsymbol{\xi}) = 4\mu\beta \Bigg\{ & \frac{1 - 2\nu}{r^3}[n_m(\mathbf{x}) n_m(\boldsymbol{\xi})\delta_{jk} + n_j(\boldsymbol{\xi}) n_k(\mathbf{x})] \\ & - \frac{1 - 4\nu}{r^3} n_j(\mathbf{x}) n_k(\boldsymbol{\xi}) + \frac{3(1 - 2\nu)}{r^5}[r_m n_m(\boldsymbol{\xi}) n_j \\ & (\mathbf{x}) r_k + r_m n_m(\mathbf{x}) r_j n_k(\boldsymbol{\xi})] + \frac{3\nu}{r^5} r_l n_l(\boldsymbol{\xi})[r_m n_m(\mathbf{x})\delta_{jk} + r_j n_k(\mathbf{x})] \\ & + \frac{3\nu}{r^5} r_k [n_m(\mathbf{x}) n_m(\boldsymbol{\xi}) r_j + r_m n_m(\mathbf{x}) n_j(\boldsymbol{\xi})] - \frac{15}{r^7} r_m n_m(\mathbf{x}) r_l n_l(\boldsymbol{\xi}) r_j \\ & r_k \Bigg\} \end{aligned}$$

The integrals of Eqs. (1), (4) can be evaluated at any point outside of the surface S. The case of $\mathbf{x} \in S$ is considered as the limiting one in which, after the evaluation of the integrals, the point $\mathbf{x}$ is allowed to reach the crack or the borehole surface.

In the problem considered, the traction on the boundary S are prescribed. Therefore, the unknown boundary values are those of the displacements on S_b and the displacements jumps on S_c. To determine these unknowns, the standard "limit after discretization" numerical procedure is employed in which the surfaces S_b and S_c are discretized, the unknown quantities are approximated, the integrals are evaluated, the limit to the boundary is taken, and the system of linear algebraic equations is set by collocation to match the limit values with the prescribed boundary data. After the algebraic system is solved, the elastic fields can be found from Eqs. (1), (4) in which all boundary data are known.

In the following Section we discuss the specific details related to that procedure.

3. Numerical procedure

The basic steps of the numerical procedure presented below are similar to those reported in [11] for crack problems. New developments are related to the introduction of the borehole in the system. Therefore, main focus of the following subsections is in the modifications needed to accommodate the integrals related to the boundary of the borehole S_b. However, for consistency (and to fix minor misprints), we provide the details related to the integration over S_c (previously reported in [11]) in Appendix A.

3.1. Notations and approximations of the geometry

In the present work, as in [11], the boundaries are approximated by a set of planar triangular elements. The element E_s is associated with a local Cartesian coordinate system (see Fig. 2) in which the basis vector $\hat{\mathbf{e}}_1$ of the system is chosen to be parallel to the side between two specifically chosen vertices of the element. The basis vector $\hat{\mathbf{e}}_3$ is chosen to be equal to $-\mathbf{n}(\boldsymbol{\xi})$, and the basis vector $\hat{\mathbf{e}}_2 = \hat{\mathbf{e}}_3 \times \hat{\mathbf{e}}_1$ is chosen in such a way that the basis $\hat{\mathbf{e}}_1\hat{\mathbf{e}}_2\hat{\mathbf{e}}_3$ is right-handed. The origin of this coordinate system may be chosen arbitrarily.

Following [11], we introduce several combinations associated with the vector $\mathbf{r}$ that connects the point $\boldsymbol{\xi}(\xi_1, \xi_2, \xi_3) \in E_s$ and the field point $\mathbf{x} = (x_1, x_2, x_3)$ as follows:

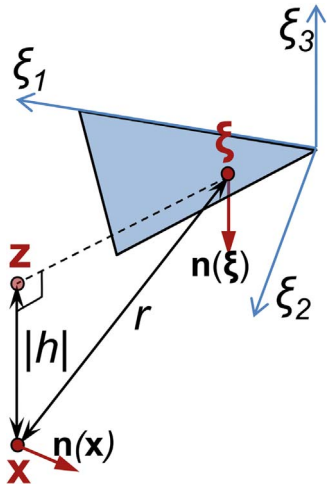

Fig. 2. Boundary element. Local coordinate system.

$$z = x_1 + ix_2 \quad \tau = \xi_1 + i\xi_2, \quad h = \xi_3 - x_3 \tag{5}$$

where $i^2 = -1$, and components of vectors are given in the local coordinate system of E_s. With notations (5) the distance r can be expressed as follows:

$$r = \sqrt{(\tau - z)(\bar{\tau} - \bar{z}) + h^2} \tag{6}$$

where $\bar{z}$ defines the complex conjugate of z, i.e. $\bar{z} = x_1 - ix_2$

As in [11], we introduce the following complex combinations of the geometry:

$$\tau - z = (\xi_1 - x_1) + i(\xi_2 - x_2) \tag{7}$$

$$\underline{n}(\mathbf{x}) = n_1(\mathbf{x}) + in_2(\mathbf{x}), \quad n_{\mathbf{n}} = n_3 \tag{8}$$

where $\mathbf{n}(\mathbf{x})$ is the normal vector to the plane containing the point $\mathbf{x}$.

Considering $\bar{\tau} - \bar{z}$ and $\tau - z$ as new independent complex variables, we can introduce the following transformation:

$$\begin{aligned} r_1 &= \xi_1 - x_1 \\ &= \frac{(\tau - z) + (\bar{\tau} - \bar{z})}{2} r_2 \\ &= \xi_2 - x_2 \\ &= \frac{(\tau - z) - (\bar{\tau} - \bar{z})}{2i} r_3 \\ &= \xi_3 - x_3 \\ &= h \end{aligned} \tag{9}$$

Similarly, we introduce the complex combinations of tractions and displacements:

$$\begin{aligned} &\underline{t} = t_1 + it_2, \quad \bar{t} = t_1 - it_2, \quad t_{\mathbf{n}} = t_3, \\ &\underline{u} = u_1 + iu_2, \quad \bar{u} = u_1 - iu_2, \quad u_{\mathbf{n}} = u_3 \end{aligned} \tag{10}$$

3.2. Approximations of the unknowns

Using the above notations we introduce a quadratic approximations of the unknown displacements and displacement discontinuities. Let us start from general polynomial expression for quadratic function $\psi^{(N)}(\xi_1, \xi_2)$ written in the Cartesian coordinate system (ξ_1, ξ_2) of the triangular element with 6 nodal points, (shown in Fig. 3) as follows:

$$\psi^{(N)}(\xi_1, \xi_2) = A_0^{(N)} + A_1^{(N)}\xi_1 + A_2^{(N)}\xi_2 + A_3^{(N)}\xi_1^2 + A_4^{(N)}\xi_2^2 + A_5^{(N)}\xi_1\xi_2 \tag{11}$$

The coefficients $A_j^{(N)}$ are obtained from the conditions that $\psi^{(N)}(\xi_1, \xi_2)$ takes a unit value at the node N, and is zero at all other nodes (Lagrange polynomial). With the use of notations (9), (11) can be

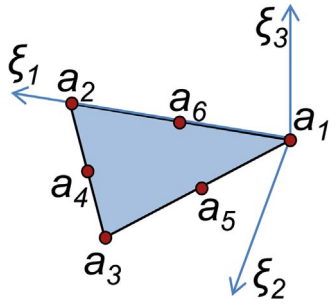

Fig. 3. Boundary element. Locations of the nodal points.

expressed in complex form as

$$\psi^{(N)}(\tau, \bar{\tau}) = \sum_{\substack{m,n=0 \\ m+n\le 2}}^{2} \kappa_{mn}^{(N)} (\tau - z)^m (\bar{\tau} - \bar{z})^n \tag{12}$$

where τ and $\bar{\tau}$ are independent variables, m, n come from the respective monomials of shape function associated with the N-th node, $\kappa_{mn}^{(N)} = \overline{\kappa_{nm}^{(N)}}$ can be obtained from $A_j^{(N)}$ and are defined by the layout of the nodes on the element E_s.

Using this definition of the shape functions, we can now approximate the displacement or displacement discontinuity vector $\Delta\mathbf{u}(\xi_1, \xi_2)$ as follows:

$$\Delta\mathbf{u} = \sum_{N=1}^{6} \Delta\mathbf{u}^{(N)} \sum_{\substack{m,n=0 \\ m+n\le 2}}^{2} \kappa_{mn}^{(N)} (\tau - z)^m (\bar{\tau} - \bar{z})^n \tag{13}$$

3.3. Contribution of an element to the discretized Eq. (1)

Here, the contribution of the element E_s into the fields described by Eq. (1) will be evaluated. Substituting the shape function of Eq. (10) into the first integral of Eq. (1) (single layer potential), we obtain the following contribution of that potential in the displacement combination $\underline{u}(\mathbf{x}) = u_1(\mathbf{x}) + iu_2(\mathbf{x})$:

$$\begin{aligned} \underline{u}^{(S)}(\mathbf{x}) = \frac{\beta}{\mu} \sum_{N=1}^{6} \sum_{\substack{m,n=0 \\ m+n\le 2}}^{2} \kappa_{mn}^{(N)} \{ [hI_{m+1,n,3}] t_{\mathbf{n}}^{(N)} \} \\ + \left[\frac{1}{2} I_{m,n,1} - \frac{h^2}{2} I_{m,n,3} \right] \underline{t}^{(N)} + [(3-4\nu) I_{m,n,1} + \frac{1}{2} I_{m+2,n,3}] \bar{t}^{(N)} \Bigg\} \end{aligned} \tag{14}$$

where the superscript (N) denotes the N-th nodal value of the corresponding boundary variable and

$$I_{m,n,k} = I_{n,m,k}^{-} = \int_{E_s} \frac{(\tau - z)^m (\bar{\tau} - \bar{z})^n}{r^k} dS_{\xi}, \quad k = 1, 3, 5, 7 \tag{15}$$

The contribution of the double layer potential (second integral of Eq. (1)) associated with the element E_s to the same displacement combination is

$$\begin{aligned} \underline{u}^{(D)}(\mathbf{x}) = \frac{2\beta}{\mu} \sum_{N=1}^{6} \sum_{\substack{m,n=0 \\ m+n\le 2}}^{2} \kappa_{mn}^{(N)} \{ [-(1-2\nu) I_{m+1,n,3}] \\ + 3h^2 I_{m+1,n,5}] \Delta u_{\mathbf{n}}^{(N)} \\ + \left[(1-4\nu) \frac{h}{2} I_{m,n,3} - \frac{3h^3}{2} I_{m,n,5} \right] \Delta\underline{u}^{(N)} \\ + [\frac{3h}{2} I_{m+2,n,5}] \Delta\bar{u}^{(N)} \} \end{aligned} \tag{16}$$

The corresponding contributions to the component u_3 are

- Single layer potential

$$u_3^{(S)} = \frac{\beta}{\mu}\sum_{N=1}^{6}\sum_{\substack{m,n=0\\ m+n\le 2}}^{2}\kappa_{mn}^{(N)}\{[(3-4\nu)I_{m,n,1}] + h^2 I_{m,n,3}]t_{\mathbf{n}}^{(N)} + [\tfrac{h}{2}I_{m,n+1,3}]\underline{t}^{(N)} + [\tfrac{h}{2}I_{m+1,n,3}]\bar{t}^{(N)}\} \quad (17)$$

- Double layer potential

$$u_3^{(D)} = \frac{2\beta}{\mu}\sum_{N=1}^{6}\sum_{\substack{m,n=0\\ m+n\le 2}}^{2}\kappa_{mn}^{(N)}\{[-h(1-2\nu)I_{m,n,3}] + 3h^3 I_{m,n+1,5}]\Delta u_{\mathbf{n}}^{(N)} + [\tfrac{(1-2\nu)}{2}I_{m,n+1,3} + \tfrac{3}{2}h^2 I_{m,n+1,5}]\Delta\underline{u}^{(N)} + \left[\tfrac{(1-2\nu)}{2}I_{m+1,n,3} + \tfrac{3h^2}{2}I_{m+1,n,5}\right]\Delta\bar{u}^{(N)}\} \quad (18)$$

3.4. Contribution of an element to the discretized Eq. (4)

By substituting the shape function of Eq. (10) into Eq. (4), the contribution of the element E_s into the adjoint double layer potential associated with the singular kernel $\mathbf{T}$ can be obtained. By choosing $\mathbf{n}(\mathbf{x})$ parallel to each of the coordinate axes, the components of the stress tensor at the point $\mathbf{x}$ can be obtained.

Here, similarly to [11], we consider the tractions associated with components of $\mathbf{n}(\mathbf{x})$ combined as suggested by Eq. (8). The resulting combinations of stresses, two of which are complex-valued and the other two are real-valued, can be used either to evaluate the traction at a collocation point or to calculate stresses inside the domain. Note that to complete both procedures, the corresponding limits to the boundary must be also evaluated (see Section 3.6). After substituting the shape function of Eq. (10) into Eq. (4), the contributions of the element E_s into the adjoint double layer potential associated with the singular kernel $\mathbf{T}$ are as follows:

$$t^{(1)}(\mathbf{x}) = \sigma_{13}(\mathbf{x}) + i\sigma_{23}(\mathbf{x}) = 2\beta\sum_{N=1}^{6}\sum_{\substack{m,n=0\\ m+n\le 2}}^{2}\kappa_{mn}^{(N)}\{-[(1-2\nu)I_{m+1,n,3}] + 3h^2 I_{m+1,n,5}]t_{\mathbf{n}}^{(N)} + \left[-\tfrac{h(5-4\nu)}{2}I_{m,n,3} + \tfrac{3h^3}{2}I_{m,n,5}\right]\underline{t}^{(N)} - [\tfrac{3h}{2}I_{m+2,n,5}]\bar{t}^{(N)}\} \quad (19)$$

$$t^{(2)}(\mathbf{x}) = \sigma_{11}(\mathbf{x}) - \sigma_{22}(\mathbf{x}) + 2i\sigma_{12}(\mathbf{x}) = 2\beta\sum_{N=1}^{6}\sum_{\substack{m,n=0\\ m+n\le 2}}^{2}\kappa_{mn}^{(N)}\{-[3hI_{m+2,n,5}]t_{\mathbf{n}}^{(N)} - [2(1-2\nu)I_{m+1,n,3} + \tfrac{3}{2}I_{m+2,n+1,5}]\underline{t}^{(N)} - [\tfrac{3}{2}I_{m+3,n,5}]\bar{t}^{(N)}\} \quad (20)$$

$$t^{(3)}(\mathbf{x}) = \sigma_{11}(\mathbf{x}) + \sigma_{22}(\mathbf{x}) = 2\beta\sum_{N=1}^{6}\sum_{\substack{m,n=0\\ m+n\le 2}}^{2}\kappa_{mn}^{(N)}\{[-h(1+4\nu)I_{m,n,3}] + 3h^3 I_{m,n,5}]t_{\mathbf{n}}^{(N)} - [\tfrac{3}{2}I_{m+1,n+2,5}]\underline{t}^{(N)} - [\tfrac{3}{2}I_{m+2,n+1,5}]\bar{t}^{(N)}\} \quad (21)$$

$$t^{(4)}(\mathbf{x}) = \sigma_{33}(\mathbf{x}) = 2\beta\sum_{N=1}^{6}\sum_{\substack{m,n=0\\ m+n\le 2}}^{2}\kappa_{mn}^{(N)}\{-[h(1-2\nu)I_{m,n,3}] + 3h^3 I_{m,n,5}]t_{\mathbf{n}}^{(N)} + [\tfrac{(1-2\nu)}{2}I_{m,n+1,3} - \tfrac{3}{2}h^2 I_{m,n+1,5}]\underline{t}^{(N)} + [\tfrac{(1-2\nu)}{2}I_{m+1,n,3} - \tfrac{3}{2}h^2 I_{m+1,n,5}]\bar{t}^{(N)}\} \quad (22)$$

The contributions of the same element into the hypersingular potential (second integral of Eq. (4)) are reported in [11]; for consistency (and to fix a minor misprint) the results are reproduced in Appendix A.

3.5. Integrals Involved in Eqs. (14)–(22)

The integrals involved in above expressions can be reduced to one generic integral of the following kind:

$$I_{m,n} = I_{m,n,1} = \int_{E_s}\frac{(\tau - z)^m(\bar{\tau} - \bar{z})^n}{r}dS_{\xi} \quad (23)$$

by using differentiation over h^2

$$I_{m,n,3} = -2\frac{\partial I_{m,n}}{\partial(h^2)},$$

$$I_{m,n,5} = \frac{4}{3}\frac{\partial^2}{\partial(h^2)^2}I_{m,n},$$

$$I_{m,n,7} = -\frac{8}{15}\frac{\partial^3}{\partial(h^2)^3}I_{m,n}$$

For a triangular element, the generic integral can be evaluated analytically, see [11,15]. For consistency, the resulting expressions are provided in Appendix B.

3.6. Evaluation of boundary tractions

The combinations $t^{(1)}(\mathbf{x}) - t^{(4)}(\mathbf{x})$ are given by Eqs. (19)–(22) and (28)–(31) of Appendix A for the case when the point $\mathbf{x}$ is located outside of the crack surface. To obtain the tractions on the boundary, meet the prescribed boundary conditions, and to evaluate the unknown displacement discontinuities, it is necessary to perform a limiting procedure in which the point $\mathbf{x}$ is allowed to reach some point at that boundary. If the boundary point is located away from the element considered this procedure is unnecessary; for the case when this point belongs to the element or is located on the plane that contains it, the limits of tractions are taken assuming that $h \to 0$. Some individual integrals involved in Eqs. (28)–(31) of Appendix A may diverge when $h \to 0$, therefore it is important to take the limit after assembling all contributions involved into expressions $t^{(1)}(\mathbf{z}) - t^{(4)}(\mathbf{z})$. For $\mathbf{z} \in S_c$, the final expressions are reported in [11]; for consistency the results are reproduced in Appendix C. The corresponding expressions for $\mathbf{z} \in S_b$ are

$$t^{(1)}(\mathbf{z}) = 2\beta(1-2\nu)\sum_{N=1}^{6}\sum_{m=1}^{3}\left[\hat{U}_{mn}^{(N)} + i\hat{V}_{mn}^{(N)}\right]t_{\mathbf{n}}^{(N)}\Big|_{n=m}^{m+1} \pm 2\beta(1-\nu)\underline{t}^{(N)}\kappa_{00}^{(N)}\gamma, \quad t^{(2)}(\mathbf{z}) = \beta\sum_{N=1}^{6}\sum_{m=1}^{3}\left[(7-8\nu)\left(\hat{U}_{mn}^{(N)} + i\hat{V}_{mn}^{(N)} + \frac{5}{2}ic_m E_{mn}\kappa_{00}^{(N)}\right)\underline{t}^{(N)} + \left(\hat{X}_{mn}^{(N)} + i\hat{Y}_{mn}^{(N)}\right)\bar{t}^{(N)}\right]_{n=m}^{m+1}, \quad t^{(3)}(\mathbf{z}) = \beta\sum_{N=1}^{6}\sum_{m=1}^{3}\left[6Re\left(\hat{U}_{mn}^{(N)}\bar{t}^{(N)}\right) + iIm\left(\hat{W}_{mn}^{(N)}\bar{t}^{(N)}\right)\right]_{n=m}^{m+1} \mp 4\beta\nu t_{\mathbf{n}}^{(N)}\kappa_{00}^{(N)}\gamma, \quad t^{(4)}(\mathbf{z}) = 2\beta(2\nu-1)\sum_{N=1}^{6}\sum_{m=1}^{3}\left[Re\left(\hat{U}_{mn}^{(N)}\bar{t}^{(N)}\right) + iIm\left(\hat{V}_{mn}^{(N)}\bar{t}^{(N)}\right)\right]_{n=m}^{m+1} \pm 2\beta(1-\nu)t_{\mathbf{n}}^{(N)}\kappa_{00}^{(N)}\gamma \quad (24)$$

where "+" or "−" signs are taken depending on the direction of approach to the boundary and the rest of the adopted notations are as follows:

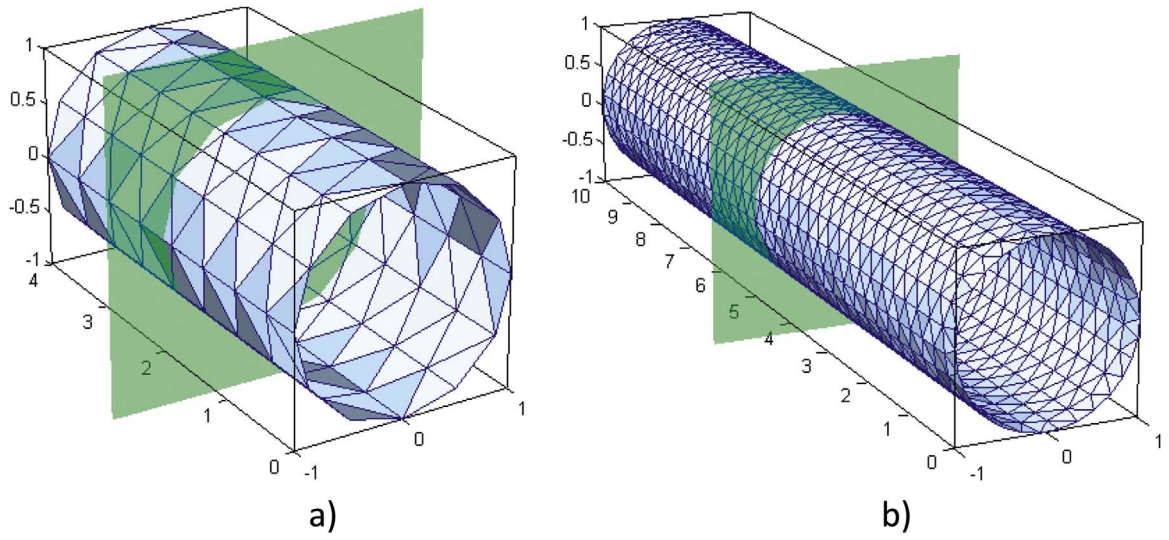

Fig. 4. Two mesh examples for a cylindrical hole: (a) $L/R = 4$, (b) $L/R = 10$.

$$
\begin{aligned}
\hat{U}_{mn}^{(N)} &= L_{mn}\,[2c_m\kappa_{00}^{(N)} + 2\,|d_m|(c_m^2\kappa_{10}^{(N)} - \kappa_{01}^{(N)}) \\
&\quad + |d_m|^2(3c_m^3\kappa_{20}^{(N)} - \bar{c_m}\kappa_{02}^{(N)} - c_m\kappa_{11}^{(N)})], \quad \hat{V}_{mn}^{(N)} \\
&= 4c_m^2\,|d_m|\,E_{mn}\kappa_{10}^{(N)} + c_m^2 P_{mn}\kappa_{20}^{(N)} + |d_m|\,\rho_n(\bar{c_m}\kappa_{02}^{(N)} + c_m\kappa_{11}^{(N)}), \quad \hat{W}_{mn}^{(N)} \\
&= 5\,|d_m|\,E_{mn}\kappa_{00}^{(N)} + 24c_m^2\,|d_m|\,E_{mn}\kappa_{10}^{(N)} + 6c_m^3 P_{mn}\kappa_{20}^{(N)} \\
&\quad + 6\,|d_m|\,\rho_n(\bar{c_m}\kappa_{02}^{(N)} + c_m\kappa_{11}^{(N)}), \quad \hat{X}_{mn}^{(N)} \\
&= c_m^2[-2c_m\kappa_{00}^{(N)} - 6\,|d_m|(c_m^2\kappa_{10}^{(N)} - \kappa_{01}^{(N)}) \\
&\quad - 3\,|d_m|^2(5c_m^3\kappa_{20}^{(N)} + \bar{c_m}\kappa_{02}^{(N)} - 3c_m\kappa_{11}^{(N)})], \quad \hat{Y}_{mn}^{(N)} \\
&= c_m^3\left(4 + \frac{1}{2}E_{mn}^2\right)\kappa_{00}^{(N)} - 4c_m^4\,|d_m|(3 - E_{mn}^2)\kappa_{10}^{(N)} + 12c_m^2\,|d_m|\,E_{mn}\kappa_{01}^{(N)} \\
&\quad - c_m^5\,|d_m|\,\rho_n(15 + 10E_{mn}^2 - 2E_{mn}^4)\kappa_{20}^{(N)} - 3c_m\,|d_m|\,\rho_n\kappa_{02}^{(N)} \\
&\quad + 3c_m^3\,|d_m|\,P_{mn}\kappa_{11}^{(N)}
\end{aligned}
\tag{25}
$$

and

$$
\begin{aligned}
L_{mn} &= \tanh^{-1}(\sin\chi_{mn}) \\
&= (\ln(1 + \sin\chi_{mn}) - \ln(1 - \sin\chi_{mn}))/2, \quad P_{mn} \\
&= 4|d_m|E_{mn} + \rho_n, \quad E_{mn} \\
&= \exp(i\chi_{mn})\gamma \\
&= \sum_{m=1}^{3}\chi_{mn}|_{n=m}^{m+1}, \quad \chi_{mn} \\
&= \arg(a_n) - \arg(d_m), \quad c_m \\
&= \frac{d_m}{|d_m|}, \quad \rho_n \\
&= \|a_n - z\| \\
&= \frac{|d_m|}{\cos\chi_{mn}}
\end{aligned}
\tag{26}
$$

where the notations for a_n and d_m are similar to those used in [15].

3.7. Linear algebraic system

The tractions at any point on the crack/borehole boundary are evaluated using standard superposition procedure in which the contributions of all elements are first transformed into the coordinate system associated with the element on which the boundary point is located and then summed up. By exactly matching the boundary tractions at the collocation points with the prescribed boundary data, the system of linear algebraic equations in terms of unknown displacement discontinuities $\Delta\mathbf{u}^{(N)}$ on S_c and displacements $\mathbf{u}^{(N)} = \mathbf{u}^{+(N)}$ on S_b is assembled (the terms that involve known tractions $\mathbf{t}^{(N)}$ are transferred to the right-hand side of the system that also includes the influence of the far-field stresses, see [11]). The positions of the collocation points are chosen following the procedure identified in [11] as "continuous approximation" scheme.

The case when cracks emanate from the borehole surface needs special attention because the displacements at the borehole boundary are continuous everywhere except the points where the crack initiates (crack mouth), while they undergo unknown jumps across the crack surface. In order to describe the jumps (displacement discontinuities) at these points, pairs of coincident nodes are introduced. Each node of the pair is associated with the borehole element located on either "+" or "−" side of the adjacent crack. While considering the crack surface element that contains these points, the difference of displacements at both nodes is considered instead of displacement discontinuity. This procedure results in additional columns (and rows) of the matrix; the integrals associated with the crack surface element adjacent to the borehole contribute to the matrix twice with opposite signs.

4. Numerical results

In this Section we illustrate the proposed approach on two examples: (i) infinite elastic space containing a uniformly pressurized borehole and (ii) two symmetrical planar cracks emanating from the borehole. As there is a lack of three-dimensional benchmark results, the choice of examples was motivated by the fact that, as expected, the stresses in the middle cross-section of a long borehole would mimic the corresponding plane strain two-dimensional stresses.

4.1. Uniformly pressurized borehole

Consider two cases of an infinite elastic medium containing a cylindrical hole that is uniformly pressurized in the radial direction and characterized by the following geometrical parameters (i) $L/R = 4$, Fig. 4a, and (ii) $L/R = 10$, Fig. 4b, where L is the length of the hole in axial direction and R is its radius.

As the length L is longer than the radius R, it is reasonable to expect (especially in the second case) that the fields in the middle cross-sections of the holes (shown on Fig. 4) would mimic the solution of the two-dimensional problem of a circular hole subjected to uniform normal load, Fig. 5. The latter problem is axisymmetric and has the following analytical solution (see [18]):

$$
\sigma_{rr}/P = -R^2/r^2, \quad \sigma_{\theta\theta}/P = R^2/r^2, \quad \sigma_{r\theta}/P = 0 \tag{27}
$$

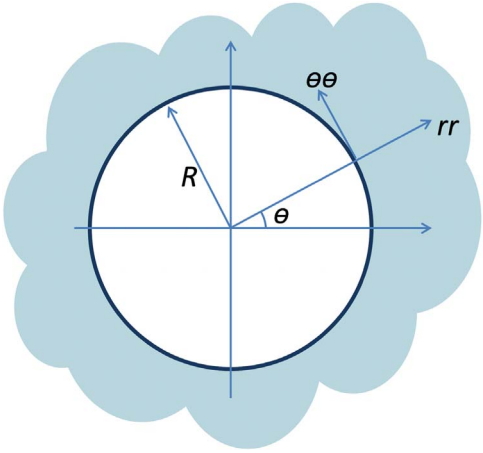

Fig. 5. A circular hole in an infinite plane.

in which P is applied pressure, r is the radial distance from the center of the circle, the angle θ is shown in Fig. 5 and σ_{rr}, $\sigma_{\theta\theta}$, $\sigma_{r\theta}$ are the stresses in the local (rotated) coordinate system.

Both three-dimensional problems were solved using quadratic approximations for the unknown boundary displacements. Three types of meshes were used to discretize cylindrical boundaries. For the first case, Fig. 4a, one mesh of 192 elements was used characterized by the ratio $h_0/R = 0.52$, in which h_0 is the characteristic length scale of the boundary elements. For the second case, Fig. 4b, the following two meshes were used: (i) $h_0/R = 0.52$ (474 elements) and (ii) $h_0/R = 0.26$ (1824 elements). In all considered cases, the pressure was applied only at the circumference of the hole and zero displacement was prescribed at its ends.

Normalized circumferential (hoop) stress $\sigma_{\theta\theta}/P$ along the radial line is plotted on Fig. 6 for the holes with both aspect ratios. The results for the case $L/R = 10$ are shown for the finer mesh only, although the coarse mesh provided quite accurate results as well. It can be seen that the hoop stress is indeed consistent with two-dimensional stress of the second equation of Eq. (25) even for the case of the hole with smaller aspect ratio L/R. The stresses evaluated on the lines with different θ should be the same and this was indeed observed with reasonable accuracy.

Normalized stress σ_{rr}/P near the hole with smaller aspect ratio computed along two radial lines is plotted on Fig. 7. While this stress should be again the same for all radial lines, the computed stress does vary with θ due to the discretization induced errors. In addition, the two-dimensional solution is not well reproduced for this aspect ratio.

The same normalized stress is plotted in Fig. 8 for the hole with larger aspect ratio discretized with both meshes. It can be seen that this stress reproduces the two-dimensional stress of the first equation of Eq. (25) quite well. The figure also illustrates mesh convergence of the solution. The results obtained for different θ are reasonably consistent.

4.2. Two symmetrical cracks emanating from a borehole

Consider an infinite elastic medium containing a cylindrical cavity representing a section of a borehole (let the axis of the borehole be the Oy axis of the coordinate system) and two symmetrical planar cracks with circular front of radius R_c and length in the radial direction of the borehole a originating from the hole parallel to its axis as shown on Fig. 9 (let yz plane be the plane of both cracks). The following geometric parameters were assumed: $L/R = 8$, $a/R = 1$, $R_c/R = 2$, in which, as before, L is the axial length of the hole, and R is its radius (thus, each crack occupies a segment of the circle with the center at the center of symmetry of the borehole). Two loading cases are considered: cracks subjected to uniform load P equal to that applied at the surface of the borehole ("slow pressurization") and traction-free cracks ("fast pressurization").

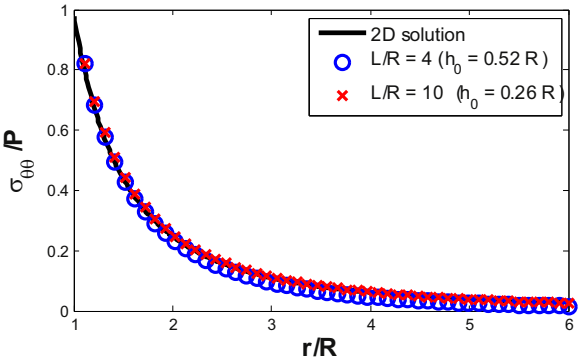

Fig. 6. Normalized hoop stress along a radial line in the middle cross-section of a borehole.

The problem was solved with quadratic approximations for the unknown displacements at the boundary of the hole and displacement discontinuities at the cracks surfaces. The used meshes were characterized by the length scale of the boundary elements h_0 (same for all boundaries) given by the ratios $h_0/R = 0.48$ (422 elements) and $h_0/R = 0.2$ (3140 elements), respectively.

Normalized stresses σ_{xx}/P, σ_{zz}/P, σ_{xz}/P along several lines (see the dashed line at angle θ with respect to the crack plane is shown on Fig. 10) in the middle cross-section of the borehole (in the plane $y = L/2$) are evaluated and compared with the corresponding stresses due to the solution of the two-dimensional problem shown on that figure. The latter problem is solved using the algorithm described in [19] that employed quadratic approximation for the unknown functions, 72 circular arc elements for the hole boundary and 12 straight elements for each of two cracks. The results are shown on Figs. 11–13 for pressurized cracks ("slow pressurization") and Figs. 14–16 for traction-free cracks ("fast pressurization"). It can be seen that reasonable qualitative agreement between two- and three-dimensional near-tip stress solutions is achieved. As we have not introduced special tip elements at this stage, we do not report the results on the three-dimensional stress intensity factors. Stress intensity factors for the corresponding two-dimensional problem have been reported in [20,21], and compared with the earlier results by Newman [22].

It cannot be expected that the two-dimensional solutions would be accurately reproduced in the fully three-dimensional setting. It appears from e.g. Fig. 11a that the stress intensity factors for the three-dimensional problems are about twice as low as for the corresponding two-dimensional problems. Rigorous studies on the stress intensity factors for the three-dimensional problem will be a subject of future research.

As expected (see e.g. [23]), higher stresses are observed in case of "slow pressurization" than in that of "fast pressurization." The shear stress vanishes with reasonable accuracy on the vertical line (Figs. 13a and 16a). The observed non-zero values are due to non-symmetrical placement of collocation points.

5. Concluding remarks

In the present paper, the boundary element-based technique introduced originally in [11,12] for crack problems is further developed to analyze borehole-cracks systems. To describe the borehole boundary, the integral representation for the tractions now involves the so-called adjoint double layer potential. The integrals associated with this potential are evaluated analytically and closed form expressions for them are reported. As in [11], approximations involve quadratic polynomials for the unknown displacements at the borehole boundary and displacement discontinuities at the crack surfaces; the boundary conditions are met using the "limit after discretization" procedure.

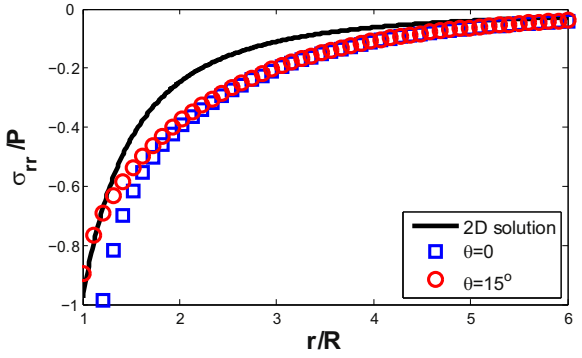

Fig. 7. Normalized radial stress σ_{rr}/P along two radial lines in the middle cross-section of a borehole for the case $L/R = 4$.

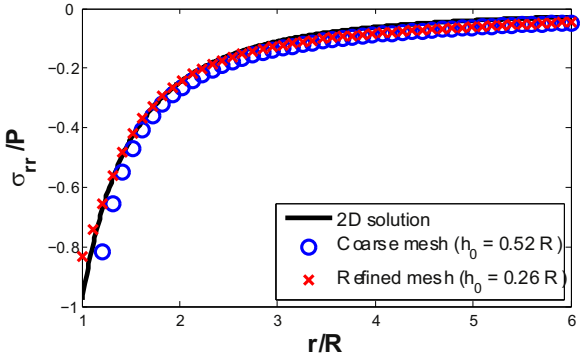

Fig. 8. Normalized radial stress σ_{rr}/P along a radial line in the middle cross-section of a borehole for the case $L/R = 10$.

Therefore, the procedure involves no singular integrals. The approach allows for using the same procedure to set up the system of linear algebraic equations for the boundary unknowns and to evaluate the elastic fields outside of the boundaries. The case of cracks emanating from the borehole is treated with the use of the pairs of coincident nodes where each node is associated with the borehole element located on either "+" or "−" side of the adjacent crack. Three benchmark numerical examples are presented to validate the approach.

Computational cost associated with the three-dimensional problems of the kind considered here is quite high. Therefore, future work will be concerned with the efficient assembly of the matrix of the linear algebraic system with the use of parallel computing (partly implemented in the computer code used for the reported simulations) and the solution of this system via available fast solvers. The further developments will include incorporation of fluid flow, e.g. the models described in [8,10], into the computer code. This work is in progress.

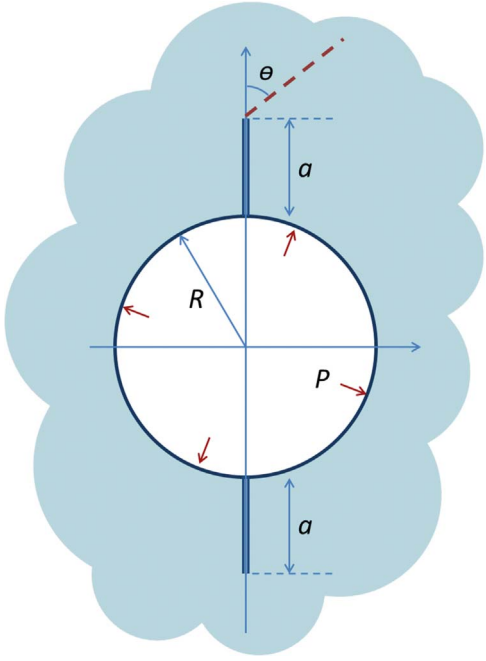

Fig. 10. Two cracks emanating from a circular hole in an infinite plane.

Acknowledgments

The third author gratefully acknowledges support from the Theodore W. Bennett Chair, University of Minnesota. Special thanks to professor Adarsh Krishnamurthy for helpful guidance on the use of parallel computing.

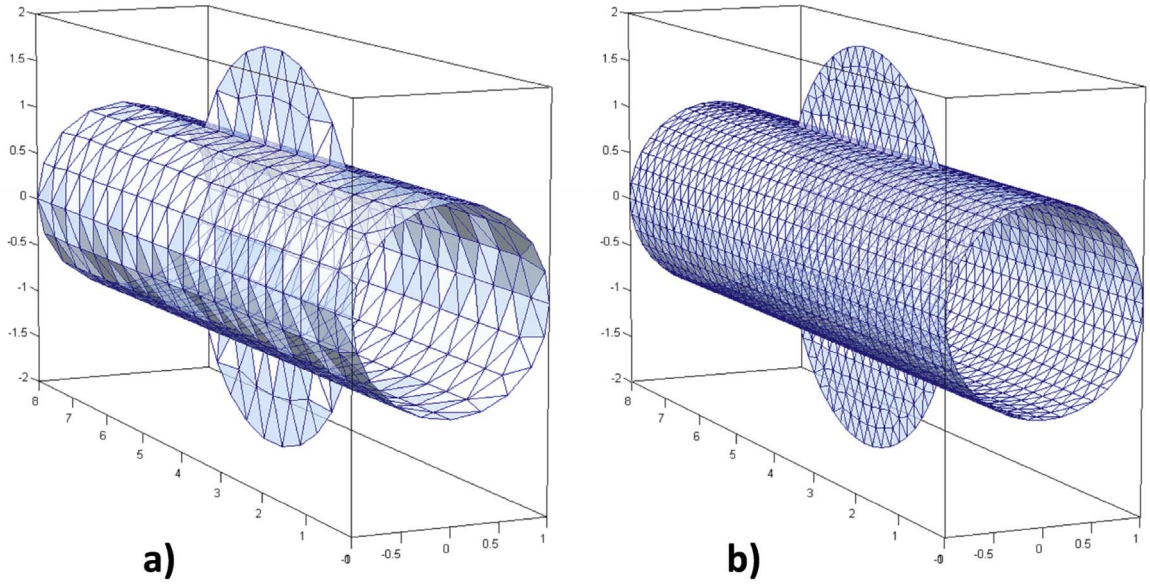

Fig. 9. Two planar cracks emanating from a borehole. Two examples of boundary mesh: (a) $h_0/R = 0.48$; (b) $h_0/R = 0.2$.

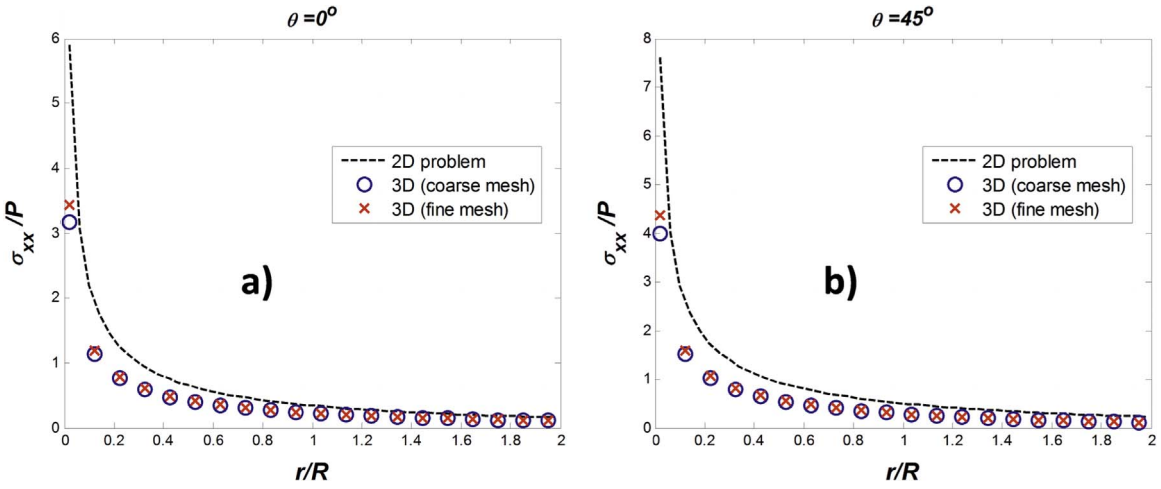

Fig. 11. Normalized stress σ_{xx}/P in the middle cross-section of a borehole with two pressurized emanating cracks.

Appendix A. Contribution of an element to the hypersingular potential of the discretized Eq. (4)

The contributions of the hypersingular kernel of Eq. (4) into the tractions at the point $\mathbf{x}$ (combined in a similar way as in Eqs. (19)–(22)) are as follows:

$$
\begin{aligned}
&t^{(1)}(\mathbf{x}) = \sigma_{13}(\mathbf{x}) + i\sigma_{23}(\mathbf{x}) \\
&= \frac{\mu}{4\pi(1-\nu)} \sum_{N=1}^{6} \sum_{\substack{m,n=0 \\ m+n\le 2}}^{2} \kappa_{mn}^{(N)} \{ [-6hI_{m+1,n,5}] \} \\
&+ 30h^3 I_{m+1,n,7}] \Delta u_n^{(N)} \\
&+ [\tfrac{(\nu-2)}{2} I_{m,n,3} - \tfrac{3}{2} h^2(\nu-5) I_{m,n,5} - \tfrac{15}{2} h^4 I_{m,n,7}] \, \underline{\Delta u}^{(N)} \\
&+ [-3\nu I_{m+2,n,5} + 15h^2 I_{m+2,n,7}] \, \bar{\Delta u}^{(N)} \}
\end{aligned} \tag{28}
$$

$$
\begin{aligned}
&t^{(2)}(\mathbf{x}) = \sigma_{11}(\mathbf{x}) - \sigma_{22}(\mathbf{x}) + 2i\sigma_{12}(\mathbf{x}) \\
&= \frac{\mu}{4\pi(1-\nu)} \sum_{N=1}^{6} \sum_{\substack{m,n=0 \\ m+n\le 2}}^{2} \kappa_{mn}^{(N)} \{ [3(2\nu-1) I_{m+2,n,5}] \} \\
&+ 15h^2 I_{m+2,n,7}] \Delta u_n^{(N)} \\
&+ [-6h\nu I_{m+1,n,5} - \tfrac{15}{2} h I_{m+2,n+1,7}] \, \underline{\Delta u}^{(N)} \\
&+ [\tfrac{15}{2} h I_{m+3,n,7}] \, \bar{\Delta u}^{(N)} \}
\end{aligned} \tag{29}
$$

$$
\begin{aligned}
&t^{(3)}(\mathbf{x}) = \sigma_{11}(\mathbf{x}) + \sigma_{22}(\mathbf{x}) \\
&= \frac{\mu}{4\pi(1-\nu)} \sum_{N=1}^{6} \sum_{\substack{m,n=0 \\ m+n\le 2}}^{2} \kappa_{mn}^{(N)} \{ [-(1+2\nu) I_{m,n,3}] \} \\
&+ 6h^2(\nu+2) I_{m,n,5} - 15h^4 I_{m,n,7}] \Delta u_{\mathbf{n}}^{(N)} \\
&+ [3h(\nu-1) I_{m,n+1,5} + \tfrac{15}{2} h I_{m+1,n+2,7}] \, \underline{\Delta u}^{(N)} \\
&+ [3h(\nu-1) I_{m+1,n,5} + \tfrac{15}{2} I_{m+2,n+1,7}] \, \bar{\Delta u}^{(N)} \}
\end{aligned} \tag{30}
$$

$$
\begin{aligned}
&t^{(4)}(\mathbf{x}) = \sigma_{33}(\mathbf{x}) \\
&= \frac{\mu}{4\pi(1-\nu)} \sum_{N=1}^{6} \sum_{\substack{m,n=0 \\ m+n\le 2}}^{2} \kappa_{mn}^{(N)} \{ [-I_{m,n,3}] \} \\
&- 6h^2 I_{m,n,5} + 15h^4 I_{m,n,7}] \Delta u_{\mathbf{n}}^{(N)} \\
&+ [-\tfrac{3}{2} h I_{m,n+1,5} + \tfrac{15}{2} h^3 I_{m,n+1,7}] \, \underline{\Delta u}^{(N)} \\
&+ [-\tfrac{3}{2} h I_{m+1,n,5} + \tfrac{15}{2} h^3 I_{m+1,n,7}] \, \bar{\Delta u}^{(N)} \}
\end{aligned} \tag{31}
$$

Appendix B. Evaluation of the generic integral (21)

For quadratic polynomial approximations of the boundary unknowns, the parameters m, n vary from 0 to 2. The closed form expression for the integral I_{mn}

$$
I_{mn} = \int_{E_s} \frac{(\tau - z)^m (\bar{\tau} - \bar{z})^n}{r} d\Sigma \tag{32}
$$

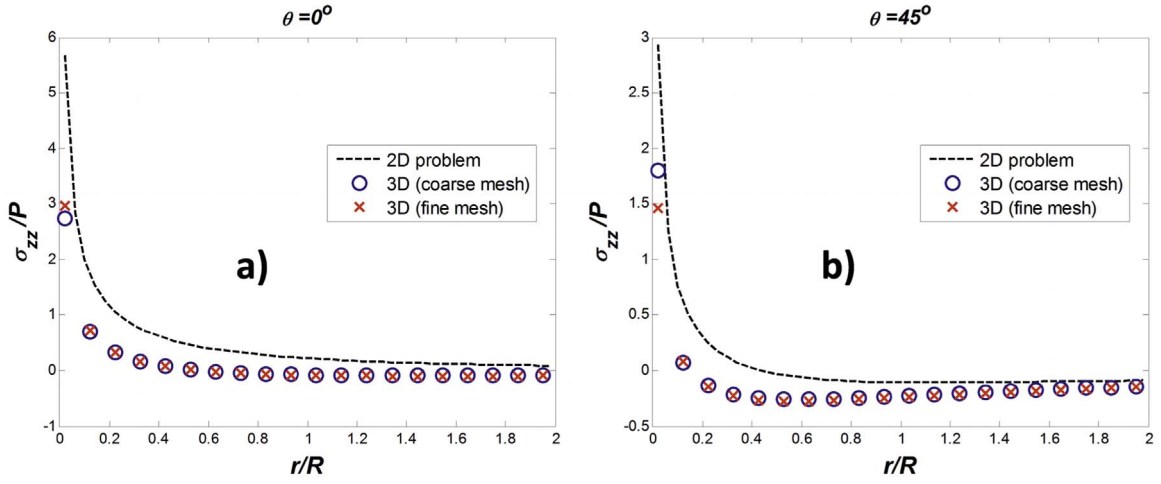

Fig. 12. Normalized stress σ_{zz}/P in the middle cross-section of a borehole with two pressurized emanating cracks.

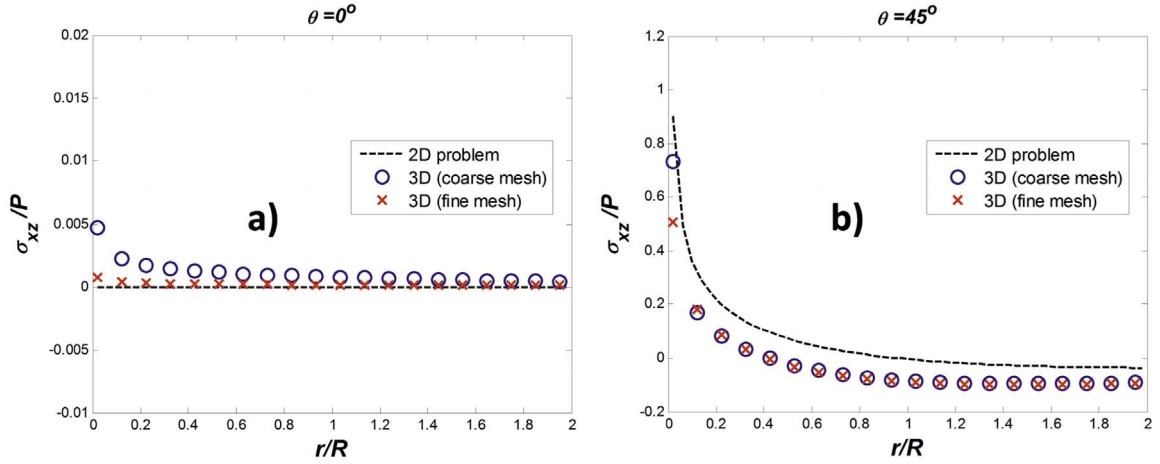

Fig. 13. Normalized stress σ_{xz}/P in the middle cross-section of a borehole with two pressurized emanating cracks.

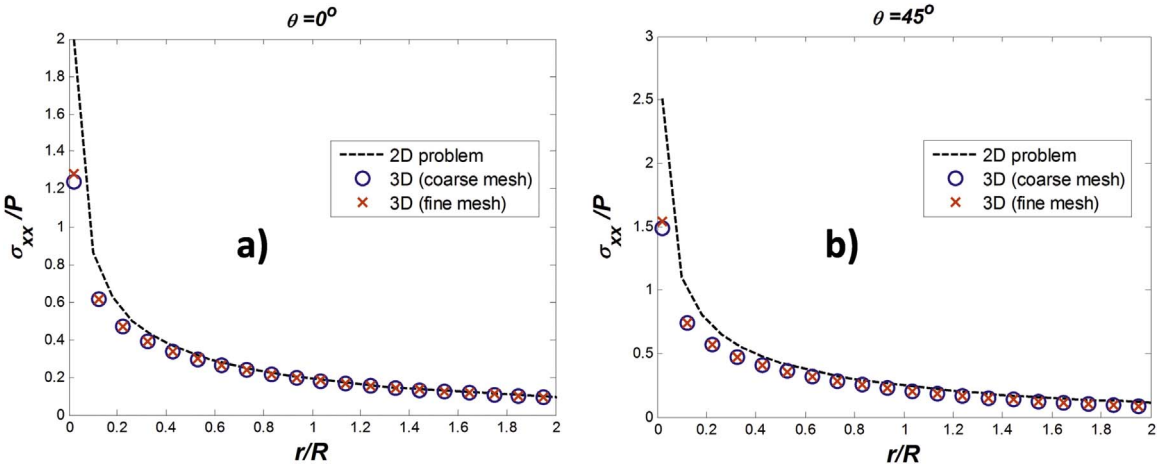

Fig. 14. Normalized stress σ_{xx}/P in the middle cross-section of a borehole with two traction-free emanating cracks.

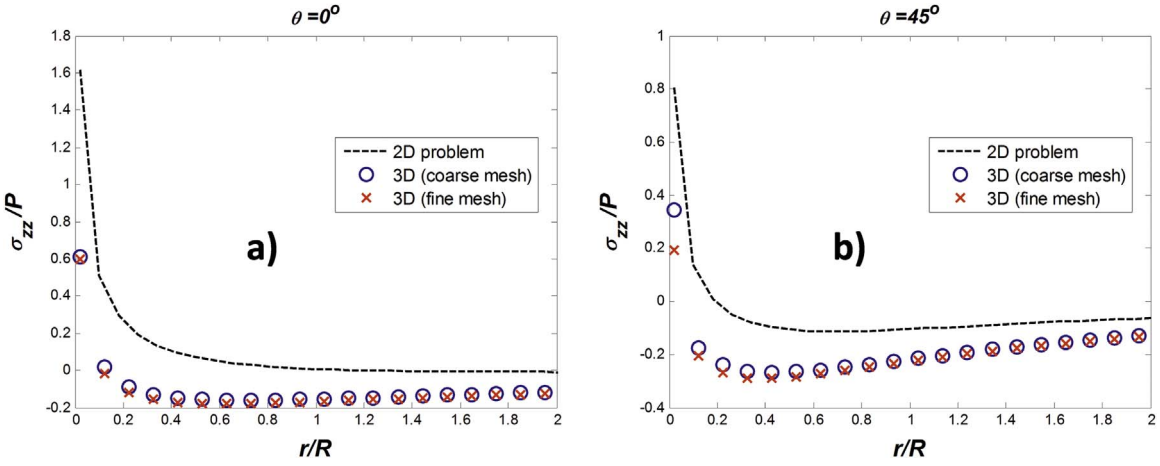

Fig. 15. Normalized stress σ_{zz}/P in the middle cross-section of a borehole with two traction-free emanating cracks.

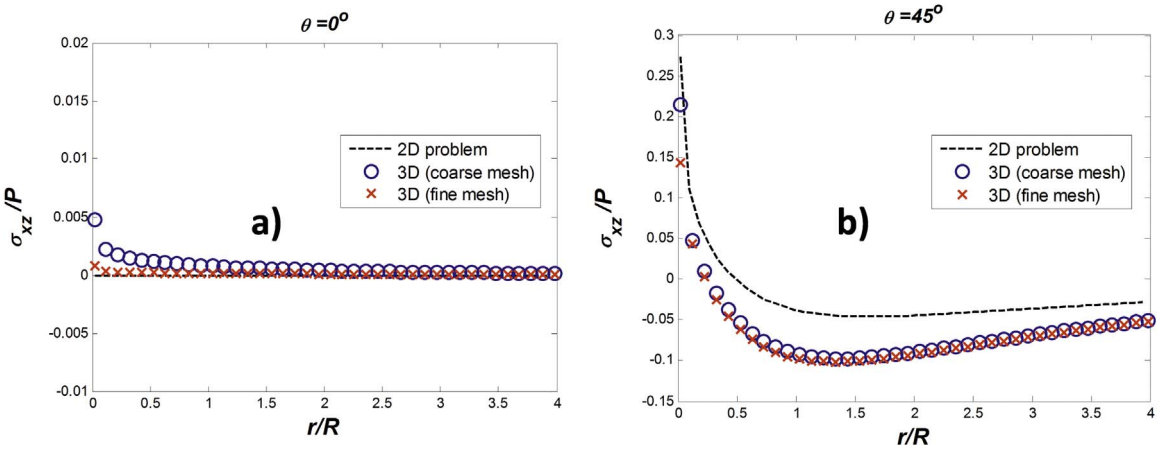

Fig. 16. Normalized stress σ_{xz}/P in the middle cross-section of a borehole with two traction-free emanating cracks.

over the triangular element E_s can be obtained as described below (see [11]):

$$
\begin{aligned}
I_{00} &= -iJ_{-1}-\begin{Bmatrix} -2\pi r & \mathbf{z}\in E_s \\ -\gamma r & \mathbf{z}\in \partial E_s \end{Bmatrix}, \quad I_{10} = -iJ_0, \quad I_{20} = -iJ_1,\\
I_{11} &= -i\tfrac{1}{3}(D_m J_1 + 2\bar{d}_m J_0 - 2h^2 J_{-1}) - \begin{Bmatrix} 2\pi h^2 & \mathbf{z}\in E_s \\ \gamma h^2 & \mathbf{z}\in \partial E_s \end{Bmatrix},\\
I_{21} &= -i\tfrac{1}{3}(D_m J_2 + 2\bar{d}_m J_1 - 2h^2 J_0),\\
I_{22} &= -i\tfrac{1}{15}[3D_m^2 J_3 + 12\bar{d}_m D_m J_2] - 4D_m(3\,|d_m|^2 + h^2)J_1\\
&\quad -8\bar{d}_m h^2 J_0 + 8h^4 J_{-1}] - \begin{Bmatrix} \frac{16}{15}\pi h^2 & \mathbf{z}\in E_s \\ \frac{8}{15}\gamma h^2 & \mathbf{z}\in \partial E_s \end{Bmatrix},
\end{aligned}
\tag{33}
$$

where $I_{mn} = \bar{I}_{nm}$ can be taken in case of $m \le n$, and for J_k one has (see [15])

$$
\begin{aligned}
J_k &= \int_{\partial E_s} r(\tau)(\tau - z)^k d\tau = \textstyle\sum_{m=1}^{3} L_{k,m},\\
L_{k,m} &= \int_{a_m}^{b_m} r(\tau)(\tau - z)^k d\tau,\\
L_{-1,m} &= -[|d_m|\, H_0 + |h|\, G_0]_{\tau=a_m}^{b_m},\\
L_{0,m} &= \tfrac{1}{2}[r d_m + C_m(|d_m|^2 + h^2)H_0]_{\tau=a_m}^{b_m},\\
L_{k,m} &= \tfrac{\bar{D}_m}{k+2}\{[r^3(\tau - z)^{k-1}]_{\tau=a_m}^{b_m}\}\\
&\quad - (2k+1)\bar{d}_m L_{k-1,m} - (k-1)h^2 L_{k-2,m}\}, \quad k \ge 1
\end{aligned}
\tag{34}
$$

In the above equations, D_m and C_m denote the following expressions:

$$
D_m = \frac{\bar{b}_m - \bar{a}_m}{b_m - a_m}, \quad C_m = \frac{b_m - a_m}{|b_m - a_m|}
$$

in which a_m, b_m are, respectively, the complex variables associated with beginning point $\mathbf{a}_m$ and the end point $\mathbf{b}_m$ of each side of the triangle (see [15]). The expressions for the other parameters involved in (33)–(34) are

$$
\begin{aligned}
d_m &= d_{1m} + i d_{2m} = \tfrac{1}{2}[a_m - z - \bar{D}_m(\bar{a}_m - \bar{z})],\\
\frac{\gamma}{2\pi} &= \begin{Bmatrix} \frac{1}{2} & \textit{for regular points} \\ \gamma_k & \textit{for } k\textit{-th corner points} \end{Bmatrix}
\end{aligned}
\tag{35}
$$

where $\gamma_k \pi$, $0 < \gamma_k \le 2$, $(k = 1,\ldots,M)$ is an internal angle at the corner point of the piecewise smooth curve ∂S, M=0 for smooth curves. The functions H_0, G_0, involved in (32), are given by the following expressions (see [15]):

$$
\begin{aligned}
H_0 &= \begin{Bmatrix} \tan^{-1}\left(\frac{|d_m|(d_m - \tau + z)}{r d_m}\right) & z \notin [a_m, b_m] \\ \sinh^{-1}\left(\frac{\tau - z}{|h|}\right) & z \in (a_m, b_m) \end{Bmatrix},\\
G_0 &= \begin{Bmatrix} \tanh^{-1}\left(\frac{|h|(d_m - \tau + z)}{r d_m}\right) & z \notin [a_m, b_m] \\ \ln\left(\frac{r + |h|}{|\tau - z|}\right) & z \in (a_m, b_m) \end{Bmatrix}
\end{aligned}
\tag{36}
$$

Appendix C. Contribution of an element to the hypersingular potential: the boundary tractions

The limit expressions for Eqs. (28)–(31) are as follows:

$$
\begin{aligned}
t^{(1)}(\mathbf{z}) &= 4\beta\mu \sum_{N=1}^{6}\left[\frac{(2-\nu)}{4}\widetilde{U}^{(N)}\underline{u}^{(N)} + \frac{\nu}{2}\widetilde{V}^{(N)}\bar{u}^{(N)}\right], \quad t^{(2)}(\mathbf{z})\\
&= 4\beta\mu \sum_{N=1}^{6}(1-2\nu)\widetilde{V}^{(N)}u_{\mathbf{n}}^{(N)}, \quad t^{(3)}(\mathbf{z})\\
&= 4\beta\mu \sum_{N=1}^{6}\frac{1+2\nu}{2}\widetilde{U}^{(N)}u_{\mathbf{n}}^{(N)}, \quad t^{(4)}(\mathbf{z})\\
&= 4\beta\mu \sum_{N=1}^{6}\widetilde{U}^{(N)}u_{\mathbf{n}}^{(N)}
\end{aligned}
\tag{37}
$$

where

$$
\begin{aligned}
\widetilde{U}^{(N)} &= \sum_{m=1}^{3}\left\{\kappa_{00}^{(N)}\frac{sin\chi_{mn}}{|d_m|} + L_{mn}(2Re(\kappa_{10}^{(N)}c_m) - \kappa_{11}^{(N)}|d_m|) + 2|d_m|\,Re,\right.\\
&\qquad \left.(\kappa_{20}^{(N)}c_m^2[L_{mn} + 2iE_{mn}])\right\}\Big|_{n=m}^{m+1}\\
&\widetilde{V}^{(N)}\\
&= \sum_{m=1}^{3}\left\{\kappa_{00}^{(N)}\frac{c_m^2}{2|d_m|}[sin\chi_{mn} - 2iE_{mn}cos\chi_{mn}] - \kappa_{10}^{(N)}\frac{c_m^3}{8}\right.\\
&\qquad [4L_{mn} + iE_{mn}(E_{mn}^2 + 8)] + \kappa_{01}^{(N)}\frac{c_m}{8}[12L_{mn} + 5iE_{mn}]\\
&\qquad - \kappa_{20}^{(N)}\frac{|d_m|\,c_m^4}{2}[3L_{mn} - 2iE_{mn}(E_{mn}^2 - 3)] - \kappa_{02}^{(N)}\frac{3|d_m|}{2}L_{mn}\\
&\qquad \left. + \kappa_{11}^{(N)}\frac{3|d_m|\,c_m^2}{2}[L_{mn} + 2iE_{mn}]\right\}\Big|_{n=m}^{m+1}
\end{aligned}
\tag{38}
$$

and L_{mn}, χ_{mn}, c_m, are defined in Eq. (11); these notations as well as $a_n$and d_m are similar to those used in [15].

References

[1] Hardy MP. Fracture mechanics applied to rocks [Ph.D thesis]. Minnesota: University of Minnesota; 1973.
[2] Abou-Sayed AS, Brechtel CE, Clifton RJ. In situ stress determination by hydro-fracturing: a fracture mechanics approach. J Geophys Res 1978;83(B6):2851–62.
[3] Atkinson C, Thiercelin M. The interaction between the wellbore and pressure-induced fractures. Int J Fract 1993;59:23–40.
[4] Carbonell R. Fracture mechanics analysis of the breakdown pressure [M.Sc thesis]. Minnesota: University of Minnesota; 1994.
[5] Detournay E, Carbonell R. Fracture mechanics analysis of the breakdown process in minifrac or leak-off tests. In: Proceedings of EUROCK 94 Symposium, Delft; 1994. p. 399–407.
[6] Mogilevskaya SG, Rothenburg L, Dusseault MB. Growth of pressure-induced fractures in the vicinity of a wellbore. Int J Fract 2000;104:L25–.
[7] Weng X. Fracture initiation from deviated wellbores. In: Proceedings of SPE 25967, presented at the 68th Annual Technical Conference and Exhibit held in Houston, TX; Oct 3–6, 1993.
[8] Adachi J, Siebrits E, Peirce A, Desroches J. Computer simulation of hydraulic fractures. Int J Rock Mech Min Sci 2007;44:739–57.
[9] Detournay E, Napier JAL. Propagation of non-planar pressurized cracks from a borehole. In: Proceedings of the Fifth International Conference on Structural Engineering, Mechanics and Computation; 2013. p. 597–602
[10] Gupta P, Duarte CA. Simulation of non-planar three-dimensional hydraulic fracture propagation. Int J Numer Anal Methods Geomech 2014:1397–430.
[11] Nikolskiy DV, Mogilevskaya SG, Labuz JF. Boundary element analysis of non-planar three-dimensional cracks using complex variables. Int J Rock Mech Min Sci 2015;76:44–54.
[12] Nikolskiy DV, Mogilevskaya SG, Labuz JF. Complex variables boundary element analysis of three-dimensional crack problems. Eng Anal Bound Elem 2013;37:1532–44.
[13] Kupradze VD. Potential methods in the theory of elasticity. Jerusalem: Israel Program for Scientific Translations; 1965. (Translation of Russian edition; 1963. Gos. Izdat. Fiz-Mat Lit, Moscow).
[14] Parton VZ, Perlin PI. Integral equations in elasticity. Moscow: Mir Publishers; 1982.
[15] Mogilevskaya SG, Nikolskiy DV. The use of complex integral representations for analytical evaluation of three-dimensional BEM integrals. Potential and elasticity problems. Q J Mech Appl Math 2014;67:505–23.
[16] Aliabadi MH. Boundary element method: applications to solids and structures, 2. Chicester, England: John Wiley & Sons, Ltd.; 2002.
[17] Mogilevskaya SG. Lost in translation: crack problems in different languages. Int J Solids Struct 2014. http://dx.doi.org/10.1016/j.ijsolstr.2014.08.025.
[18] Muskhelishvili NI. Some basic problems of the mathematical theory of elasticity – fundamental equations, plane theory of elasticity, torsion, and bending. Groningen: P. Noordhoff; 1963.
[19] Mogilevskaya SG. The universal algorithm based on complex hypersingular integral equation to solve plane elasticity problems. Comput Mech 1996;18:127–38.
[20] Mogilevskaya SG, Rothenburg L, Dusseault MB. Interaction between a circular opening and fractures originating from its boundary in a piecewise homogeneous plane. Int J Numer Anal Methods Geomech 2000;24:947–70.
[21] Jin X, Shah S, Roegiers J-C, McLennan J. Weight function of stress intensity factor for symmetrical radial cracks emanating from hollow cylinder. Eng Fract Mech 2016;159:144–54.
[22] Newman JC. An improved method of collocation for the stress analysis of cracked plates with various shaped boundaries. Report D-6376, NASA TN; 1971. p. 1–45.
[23] Detournay E, Jeffrey RG. Stress conditions for initiation of secondary fractures from a fractured borehole. In: Proceedings of the International Symposium on Rock Stress and Rock Stress Measurements, Stockholm; 1986. p. 281–288.